RSC Advances

PAPER

View Article Online
View Journal | View Issue

Cite this: *RSC Adv.*, 2017, **7**, 38677

A thermal-induced electric current from a gold electrode/porous silicon device†

Cheng-Yin Huang, Chin-Kai Chang, Kai-Shin Wen and Vincent K. S. Hsiao *

Received 15th May 2017
Accepted 22nd July 2017

DOI: 10.1039/c7ra05474b

rsc.li/rsc-advances

We demonstrate the electric current measured from a device composed of electrochemically etched silicon, porous silicon (PS) and gold (Au) electrodes of different device designs by applying a thermal potential between two Au electrodes. Compared to conventional PS of high contact resistance between Au/PS due to the homogeneously dispersed nanopores, our PS inhibits the discontinuous, island-shaped and micro-sized Si structures, which decrease the Au/PS contact resistance. When one Au electrode is heated, a temperature gradient (ΔT) is generated between the two electrodes and the electric current can be directly measured by a current meter under a close circuit condition. The output current not only depends on the electrode design but also on the distance between the electrodes. For the comb-shape electrode with finger lengths of 8 mm, widths of 0.1 mm, and finger separation of 0.14 mm, using a 25 °C setting temperature (T_{set}) can generate ΔT = 0.4 K, which corresponds to 14.2 μA. For the Au/PS device with two 16 mm^2 square electrodes separated by a 2 mm distance, the current increases with increasing T_{set} and reaches a maximum value of 25 μA corresponding to ΔT = 3.4 K. Our Au/PS device has potential in sensitive temperature sensors operated at temperatures lower than 60 °C.

Introduction

Nanostructured silicon (n-Si) with cost-effective properties, which can be easily integrated into CMOS processing, has been considered as the ultimate thermoelectric material.[1–3] Several studies have theoretically or experimentally demonstrated the enhanced thermoelectric power of n-Si from the evaluation of the Seebeck coefficient S ($S = \Delta V/\Delta T$, where ΔV and ΔT are the potential and temperature gradient between the electrode from the thermoelectric device, respectively) and figures of merit ZT (ref. 4–20) ($ZT = \sigma S^2 T/\kappa$, where σ and κ are the electrical and thermal conductivity of the material, respectively and T is the absolute temperature) due to the decrease of κ from n-Si when compared to bulk Si. Nassiopoulou *et al.*, constructed a thermoelectric device with an output thermoelectric power of 0.4 μW cm^{-2} using porous Si (PS) as a thermal isolator[21] and demonstrated the porosity-dependent Seebeck coefficient from PS[20] (1 mV K^{-1} for a 50% porosity PS). Fischer *et al.*, experimentally characterized the thermoelectric properties of nanoporous Si nanowires with a Seebeck coefficient of 1.2 mV K^{-1}.[22] Conventional evaluation of the Seebeck coefficient involves generating a temperature gradient (ΔT) and measuring the potential difference (ΔV) under an open circuit condition. In this study, we heated a gold (Au) electrode/PS junction and measured the electric current between the hot and cold junction under a close circuit condition, as shown in Fig. 1. Since the Peltier effect is described as a heating or cooling effect, which can be induced by applying currents between two electrodes connected with a thermoelectric material only under a closed circuit condition, we demonstrated a reversed Peltier effect or unconventional Seebeck effect where the generated electric current at the Au/PS junction was proportional to the heat absorbed from the device. Our experimental results show that by heating one Au/PS junction, an electric current can be directly measured using a current meter. For an Au/PS thermoelectric device with a comb-shape electrode with finger electrodes separated at a short distance (0.14 mm), a 0.4 K temperature gradient generated a 14 μA electric current. Different electrochemical etching conditions and electrode design provide different electric current behavior. Other devices, such as using square electrodes of 16 mm^2 with at least

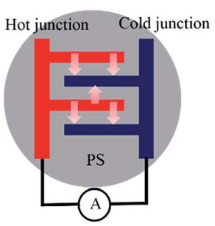

Fig. 1 A schematic of the current measurement from an Au electrode/PS junction device under close circuit conditions by heating one side of the Au electrode.

Department of Applied Materials and Optoelectronic Engineering, National Chi Nan University, Nantou, Taiwan 54561. E-mail: kshsiao@ncnu.edu.tw

† Electronic supplementary information (ESI) available. See DOI: 10.1039/c7ra05474b

1 mm separation between the two electrodes, exhibited higher ΔT values under the same heating conditions (T_{set}) controlled by a flexible heater. For an Au/PS thermoelectric device with square electrodes separated by 2 mm, a 25 μA electric current was obtained by generating $\Delta T = 3.4$ K at $T_{set} = 70$ °C.

Experimental

PS samples were prepared at room temperature *via* a wet electrochemical etching process in hydrofluoric acid (HF) using p-type boron doped single crystalline Si (with a thickness of approximately 500 μm and resistivity of 1–10 Ω cm) in (100) orientation. Electrochemical etching was performed in a home-made Teflon cell at a constant current density of 30 mA cm^{-2} for 30, 40 and 50 min in an electrolyte solution of 48 wt% HF, 98 wt% isopropanol (IPA), and deionized (DI) water. The electrolyte consisted of a HF : IPA : DI water solution with a volume ratio of 1 : 2 : 1. The control experiment for the PS sample was fabricated using an electrolyte composed of HF : ethanol = 1 : 1 (volume ratio). For each sample, the Au electrode was directly deposited onto the PS using a thermal evaporation method with a shadow mask. For the electric current measurements, an ultra-thin flexible heater (KLC Corporation, Taiwan) was attached to the backside of the PS sample and a current meter (Keithley 6485 picoamp meter with 10 fA resolution) was directly connected to the two electrodes, as shown in Fig. S1a and b.† The heating conditions (T_{set}) were controlled by setting the temperature of the heater. The current was directly recorded from the current meter under close circuit conditions without applying an external voltage. The positive (negative) value of the current was obtained by heating the Au electrode connected to the negative (positive) probe of the current meter. The ΔT between electrodes was measured using a thermal IR detector.

Results and discussion

Fig. 2 shows the surface and cross-sectional scanning electron microscopy (SEM) images of the electrochemically etched PS. A typical use of ethanol, along with HF for anodized etching of PS, is to eliminate hydrogen bubbles, making the etching process more homogeneous and generating well-dispersed nanopores inside the PS layer, as shown in Fig. 2a. However, the use of IPA facilitates inhomogeneous etching[23] and a discontinuous, micro-size and island-shape PS layer is obtained, as shown in Fig. 2b. The observed island-like shapes in the PS samples play critical roles in the photothermoelectric effect reported previously.[24] The increased island-shaped areas and decreased etching thicknesses were observed in the PS samples as the etching time increased, as shown in Fig. 2c and d. Table 1 shows the measured electric current obtained from the Au/PS junction devices with comb-shape electrode design (finger separation of 0.14 mm) using PS fabricated under different etching conditions with the same electrode heating conditions ($T_{set} = 25$ °C). For the Au/PS device using PS fabricated by conventional etching without using IPA, no evident electric current was observed; however, an enhanced electric current (14 μA) was observed from the PS samples fabricated using IPA. The

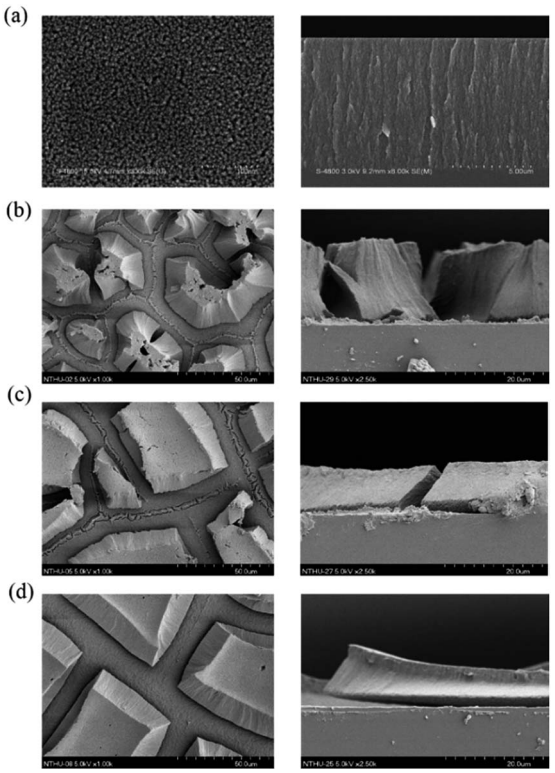

Fig. 2 The surface (left) and cross-sectional (right) SEM images of PS etched using (a) HF : ethanol = 1 : 1 and (b) HF : IPA : DI water = 1 : 2 : 1 of 30 min. (c) and (d) are the SEM images of PS etched using the IPA recipe but the etching time was 40 and 50 min, respectively. The etching current density was fixed at 30 mA cm^{-2}.

Seebeck coefficient of PS fabricated from a conventional recipe of mixed HF/ethanol was 0.6–1.0 μV K^{-1} measured in the temperature range 150–300 K.[5,20] The electrical conductivity of PS was measured to be 5–10 Ω^{-1} cm^{-1} in the same temperature range.[5] Therefore, the calculated current from the comb-shape electrode Au/PS device, in which the PS was fabricated without using IPA, was 1 nA, which is close to our measured current, as shown in Table 1. The enhanced electric current measured from the Au/PS device consisted of discontinuous, island-shape and micro-size PS may due to the decrease of contact resistance between the Au electrode and PS and the leakage current inside the PS. A previous study on the linear *I–V* characteristics[24] proved the concept of low contact resistance and the leakage current of the device. The measured current

Table 1 The thermal-induced electric current measured from a comb-shape electrode Au/PS device fabricated using different electrochemical etching conditions. T_{set} was set at 25 °C at the heater. ΔT was 0.4 K for all the samples under these heating conditions

Sample preparation conditions	TEC (μA)
HF : ethanol = 1 : 1	+0.004/−0.004
HF : IPA : DI water = 1 : 2 : 1/etching 30 min	+14.2/−10.9
HF : IPA : DI water = 1 : 2 : 1/etching 40 min	+12.2/−11.3
HF : IPA : DI water = 1 : 2 : 1/etching 50 min	+5.9/−5.2

decreased upon increasing the etching time, which may be attributed to a decrease in the thickness of the micro-sized PS layers. In addition, the amount of nanopores reduced on increasing the etching time whose effect prevented the quantum confinement of PS and further reduced the electrical conductivity inside PS. Therefore, the thermal-induced electrical current decreased with an increased etching time.

The peak intensity of the photoluminescence (PL) was observed from the PS samples etched without using IPA at 720 nm, as shown in Fig. 3a, in addition, no evident electric current was observed from that etched sample upon generating a heat potential at the two gold electrodes. The peak intensity of the PL observed from PS etched using IPA was blue-shifted to 630 nm, as shown in Fig. 3b. The blue-shifted PL may be attributed to the change in the surface morphology of the PS samples fabricated using IPA, as shown in Fig. 2. The PL intensity decreased as the electrochemical etching time increased. The measured electric current from the PS samples under the same heating conditions also decreased as the etching time increased. Previous studies[5,6] have shown that the PL and the Seebeck coefficient are affected by the porosity of PS. The Seebeck coefficient increased with increasing porosity, reached a maximal value at 51% porosity and then decreased.[20] However, no PL peak was observed from the samples of 51% porosity.[20] Herein, we observed that the maximal electric current was obtained from a sample etched for 30 min with the highest PL intensity. The PL peak wavelength was blue-shifted with an increased etching time, indicating a decrease in the crystal size of the nanocrystalline Si. Therefore, the porosity increased with increased etching time because of the decrease in the crystal size of the nanocrystalline Si. The increased porosity helped to increase the thermal conductivity value; however, the electrical conductivity decreased with increasing porosity. More investigation must be carried out to examine the dependence of the Seebeck coefficient on the surface morphology using an Au/PS simple design where the PS can be fabricated under different etching conditions, such as composition of electrolyte and etching current density.

Fig. 4 shows the T_{set}-dependent current measured from an Au/PS device using different electrode designs. T_{set} represents the temperature setting in the flexible heater attached on the bottom of the Au/PS device. The electric current suddenly increases as the setting temperature becomes larger than 26 °C, as shown in Fig. 4a. The temperature gradient (ΔT) between the two Au gold electrodes remains unchanged even upon increasing the heating temperature due to the small separation distance (0.14 mm) between the fingers. A larger finger separation (0.6 mm) helps increase the ΔT value, as shown in Fig. 4b; however, the measured electric current between the two electrodes also decreases. Using the electrode design without the use of fingers, as shown in Fig. 5b (inset), a high ΔT value was generated, but the generated electric current was comparably lower than that of the device with finger electrodes, as shown in Fig. 4c.

To verify the electrode separation-dependent current, a more simple design of the Au/PS devices were fabricated and measured. Two 4 mm × 4 mm square electrodes separated by different distances were used in the Au/PS devices, as shown in Fig. 5a (inset). When the Au electrode, which was connected to the current meter with the negative probe, was heated, a positive electric current was obtained due to the generation of ΔT between the two electrodes. The current increased with increasing heating temperature, which generated a larger

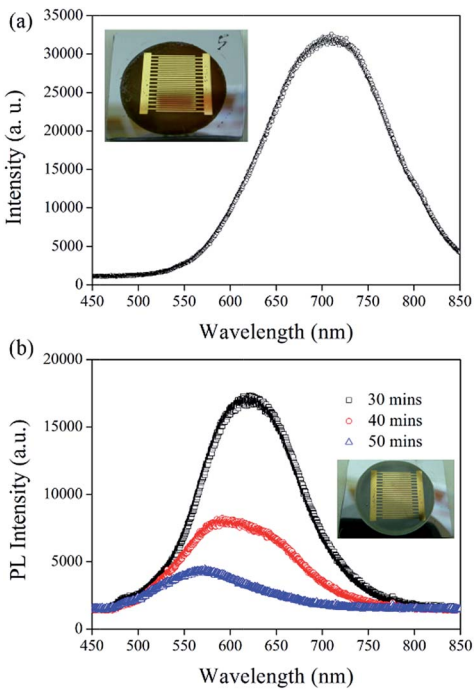

Fig. 3 The PL intensity of PS using (a) conventional etching conditions and (b) IPA etching using different etching times. The electrode design has two comb-shaped electrodes (inset) with finger lengths of 8 mm, widths of 0.1 mm and finger separation of 0.14 mm.

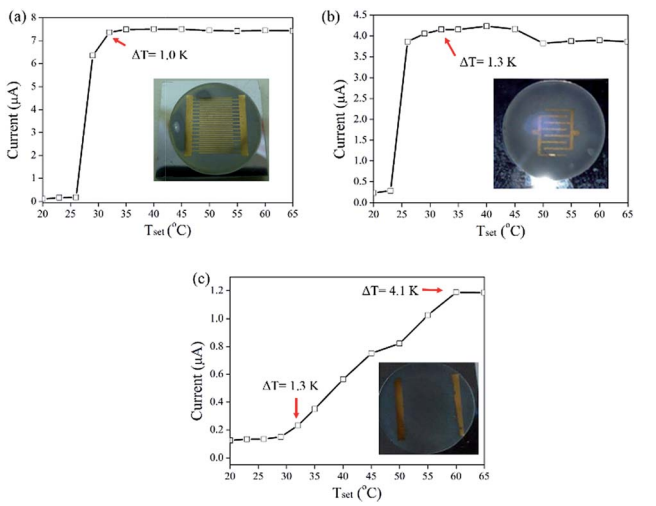

Fig. 4 The heating temperature dependence of the electric current measured in the Au/PS devices using comb-shaped electrodes with (a) finger length of 8 mm, width of 0.14 and finger separation of 0.14, (b) finger length of 4 mm, width of 0.1 mm and finger separation of 0.6 mm, and (c) strip-shaped electrodes.

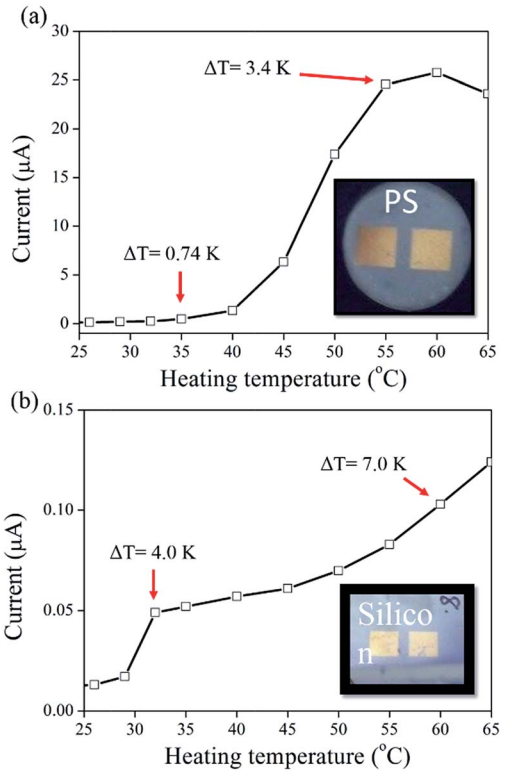

Fig. 5 The heating temperature dependence of the electric current measured in the (a) Au/PS devices with square electrodes of 16 mm^2 and (b) same electrode design but using single-crystalline Si as the substrate.

ΔT value. The current reached a maximum value of 25 μA corresponding to $\Delta T = 3.4$ K, as shown in Fig. 5a. A control sample comprising a Au/single-crystalline Si device was fabricated and measured under different heating temperatures and no evident thermal current was observed (0.10 μA) when T_{set} = 60 °C, corresponding to $\Delta T = 7$ K, as shown in Fig. 5b.

Fig. 6 shows the thermal current behaviour of the Au/PS devices with different distance between the two Au electrodes. When the setting conditions were in the range of 52–60 °C, a 2 mm separation Au/PS device had a larger thermal-induced electric current than the other devices with different electrode separation distances. The current slightly decreased or remained unchanged when the heating temperature was higher than 60 °C, as shown in Fig. 6a. A ΔT between the two electrodes was measured and the heating temperature-dependent ΔT was characterized in different devices, as shown in Fig. 6b. It is of interest that the separation between the two electrodes provided different ΔT value under the same setting temperature conditions. When the samples were measured at higher setting temperature (T_{set} > 60 °C), the same T_{set} provided higher values of ΔT in the 2 mm separation Au/PS devices, which also showed higher values for the thermal-induced current. At a moderate setting temperature range (T_{set} = 52–60 °C), a 1 mm separation Au/PS device showed a larger ΔT, which corresponds to the maximal current. At a low setting temperature range (T_{set} = 29–35 °C), a 0.5 mm separation Au/PS device had a large ΔT value and thermal-induced current, as shown in Fig. 6c.

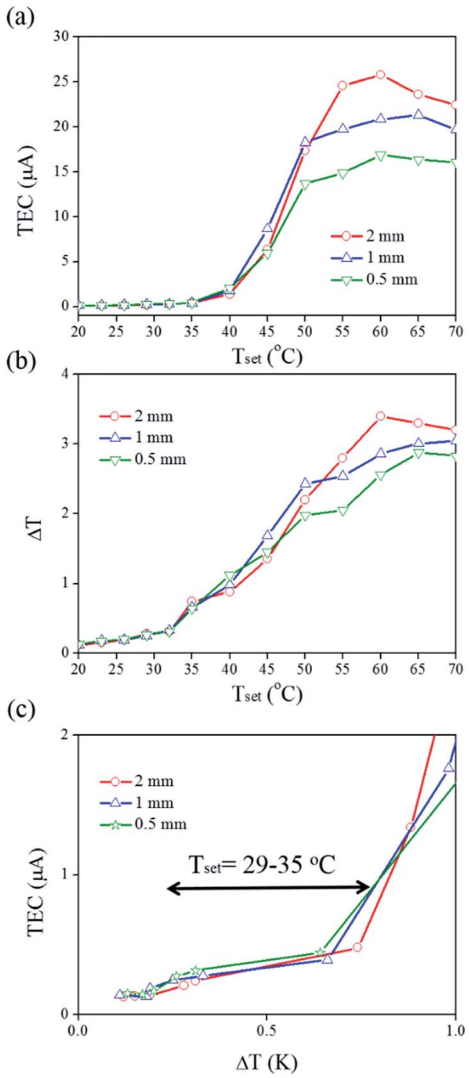

Fig. 6 (a) The thermal-induced current and (b) ΔT dependence on the setting temperature (T_{set}). (c) The ΔT-dependent electric current characterized in the Au/PS thermoelectric devices with square electrodes of 16 mm^2 with different electrode separation distances.

Conclusions

We measured the TECs generated from simple thermoelectric devices composed of Au/PS. When one electrode was heated, a thermal potential corresponding to a TEC was generated and measured in a close circuit connection. The TECs were characterized from the PS samples fabricated under different electrochemical etching conditions. A 30 min etched PS sample with the highest PL intensity and relatively thick etching thickness showed better TEC performance. Different electrode designs affected the performance levels of the Au/PS thermoelectric devices. Our demonstration is suitable for highly sensitive sensors intended for operation at low temperatures or photovoltaic–thermoelectric hybrid devices.

Acknowledgements

This study was funded by the Ministry of Science and Technology (MOST), Taiwan, under project number MOST-103-2221-E-260-016-MY3.

Notes and references

1 R. Venkatasubramanian, E. Siivola, T. Colpitts and B. O'Quinn, *Nature*, 2001, **413**, 597.
2 A. I. Boukai, Y. Bunimovich, J. Tahir-Kheli, J. K. Yu, W. A. Goddard III and J. R. Heath, *Nature*, 2008, **451**, 168.
3 A. I. Hochbaum, R. Chen, R. D. Delgado, W. Liang, E. C. Garnett, M. Najarian, A. Majumdar and P. Yang, *Nature*, 2008, **451**, 163.
4 J. L. G. Gesele, V. Drach, J. Fricke and R. Arens-Fischer, *J. Phys. D: Appl. Phys.*, 1997, **30**, 2911–2916.
5 R. G. Mathur, R. M. Mehra and P. C. Mathur, *J. Appl. Phys.*, 1998, **83**, 5855.
6 A. Yamamoto, H. Takazawa and T. Ohta, *18th International Conference on Thermoelectrics*, 1999, p. 428.
7 D. Kraemer, L. Hu, A. Muto, X. Chen, G. Chen and M. Chiesa, *Appl. Phys. Lett.*, 2008, **92**, 243503.
8 J. H. Lee, G. A. Galli and J. C. Grossman, *Nano Lett.*, 2008, **8**, 3750.
9 F. X. Alvarez, D. Jou and A. Sellitto, *Appl. Phys. Lett.*, 2010, **97**, 033103.
10 J. Tang, H. T. Wang, D. H. Lee, M. Fardy, Z. Huo, T. P. Russell and P. Yang, *Nano Lett.*, 2010, **10**, 4279.
11 N. Wang, L. Han, H. He, N.-H. Park and K. Koumoto, *Energy Environ. Sci.*, 2011, **4**, 3676.
12 D. D. Y. He, J.-H. Lee, J. C. Grossman and G. Galli, *ACS Nano*, 2011, **5**, 1839.
13 Z.-G. Chen, G. Han, L. Yang, L. Cheng and J. Zou, *Prog. Nat. Sci.: Mater. Int.*, 2012, **22**, 535.
14 N. Neophytou, X. Zianni, H. Kosina, S. Frabboni, B. Lorenzi and D. Narducci, *Nanotechnology*, 2013, **24**, 205402.
15 K. T. Park, S. M. Shin, A. S. Tazebay, H. D. Um, J. Y. Jung, S. W. Jee, M. W. Oh, S. D. Park, B. Yoo, C. Yu and J. H. Lee, *Sci. Rep.*, 2013, **3**, 2123.
16 G. H. Tang, C. Bi and B. Fu, *J. Appl. Phys.*, 2013, **114**, 184302.
17 G. Pennelli, *Beilstein J. Nanotechnol.*, 2014, **5**, 1268.
18 G. Schierning, *Phys. Status Solidi A*, 2014, **211**, 1235–1249.
19 M. J. Lee, J. H. Ahn, J. H. Sung, H. Heo, S. G. Jeon, W. Lee, J. Y. Song, K. H. Hong, B. Choi, S. H. Lee and M. H. Jo, *Nat. Commun.*, 2016, **7**, 12011.
20 K. Valalaki, P. Benech and A. Galiouna Nassiopoulou, *Nanoscale Res. Lett.*, 2016, **11**, 201.
21 E. Hourdakis and A. G. Nassiopoulou, *Sensors*, 2013, **13**, 13596.
22 G. Yuan, R. Mitdank, A. Mogilatenko and S. F. Fischer, *J. Phys. Chem. C*, 2012, **116**, 13767.
23 H. Kim and N. Cho, *Nanoscale Res. Lett.*, 2013, **7**, 408.
24 Y.-S. Lai, C.-Y. Tsai, C.-K. Chang, C.-Y. Huang, V. K. S. Hsiao and Y. O. Su, *Adv. Mater.*, 2016, **28**, 2644.